An Investigation of Shallow Water Mode Coupling Effects During Single Mode Transmission

by

Denis Peregrym

B.A.Sc., Engineering Physics, Simon Fraser University (1992)

Submitted in partial fulfillment of the
requirements for the degree of

MASTER OF SCIENCE IN ELECTRICAL ENGINEERING

at the

MASSACHUSETTS INSTITUTE OF TECHNOLOGY

and the

WOODS HOLE OCEANOGRAPHIC INSTITUTION

September 1994

Signature of Author .....
Joint Program in Applied Ocean Science and Engineering
Massachusetts Institute of Technology
Woods Hole Oceanographic Institution
August 17, 1994

Certified by .....
Josko Catipovic
Woods Hole Oceanographic Institution
Thesis Supervisor

Certified by .....
Prof. Arthur B. Baggeroer
Massachusetts Institute of Technology
Thesis Supervisor

Accepted by .....
Prof. Arthur B. Baggeroer
Chairman, Joint Committee for Applied Ocean Science and Engineering
Massachusetts Institute of Technology/Woods Hole Oceanographic Institution

An Investigation of Shallow Water Mode Coupling Effects During Single Mode Transmission

by Denis Peregrym

Submitted to the Massachusetts Institute of Technology/
Woods Hole Oceanographic Institution
Joint Program in Applied Ocean Science and Engineering
on August 17, 1994, in partial fulfillment of the requirements
for the degree of Master of Science in Electrical Engineering

Abstract

Researchers at the Woods Hole Oceanographic Institution are currently developing a method of generating acoustic fields in a shallow water coastal environment with the energy concentrated predominantly in a single mode. This method will be particularly useful for making observations of mode coupling. This thesis focuses on modelling the mode coupling associated with travelling packets of internal solitary waves, potentially one of the first applications of this technique.

A mode coupling theory based on environmental perturbations is developed which allows us to predict the coupled oscillator like behavior of the mode coupling caused by internal wave packets. Acoustic simulations using a parabolic equation based code show that we can predict whether a specific internal wave packet will cause coupling to occur, which mode pairs will be affected, and the length scale of the resulting oscillation of energy between modes. The sensitivity of these predictions to the shape and spacing of the internal waves is discussed. Simulated experimental data is generated to show that these internal waves could be detected from experimental mode coupling observations and parameters such as speed of propagation, wave height and spacing, and packet length could also be determined.

Thesis Supervisor: Josko Catipovic
Woods Hole Oceanographic Institution

Thesis Supervisor: Prof. Arthur B. Baggeroer
Massachusetts Institute of Technology

This page left blank.

Contents

List of Tables

List of Figures

This page left blank.

Chapter 1

Introduction

The propagation of acoustic waves in the underwater environment can be described by the Helmholtz equation. In cases where the environmental parameters of sound speed and density vary with depth only, the Helmholtz equation separates and the solution of the depth equation is a weighted sum of orthonormal functions. We usually refer to this set of functions as the normal modes of the waveguide. These modes are not simply a mathematical abstraction — they are physical in the sense that each mode describes an acoustic disturbance which propagates through the environment completely independently of all the others.

Range dependence in the environment means that the Helmholtz equation no longer separates and the modes cease to propagate independently. The modes interact with each other, exchanging energy in a process we call coupling. In fact, one would be correct to say that, by their definition both mathematically as a separated depth solution and physically as independently propagating acoustic disturbances, the modes no longer exist. Nevertheless, because the mode functions form a complete orthonormal set, their weighted sum can still represent the acoutic field. In cases where the range dependence is weak or regular this mathematical representation of interacting modes, which we call coupled mode theory, can be very useful.

1.1 Single Mode Transmissions

Researchers at the Woods Hole Oceanographic Institution (WHOI) are currently developing a method of generating acoustic fields in a shallow-water coastal environment with the energy concentrated predominantly in a single mode [1]. As Figure 1-1

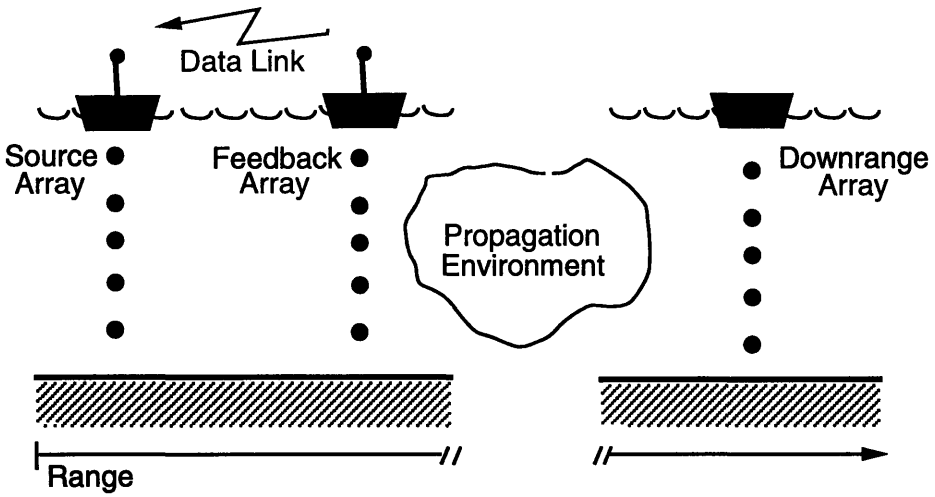

Figure 1-1: Schematic Diagram of WHOI's Single Mode Generation Technique

shows, this technique uses information from a feedback array to adjust the source array weights. As a result, the field at the feedback array is composed with as much energy as possible in the selected starting mode. Then observations made downrange from the feedback array directly give the mode coupling caused by the environment through which the acoustic field has propagated.

The first experiment in this research program, scheduled for the fall of 1994, is designed to test our ability to concentrate the transmitted acoustic energy in a single mode and will be conducted in an area which is approximately range independent. The next step, however, will be to use this ability to observe and parameterize the range dependence of the environment from the coupling which occurs from the (originally) single mode.

Many forms of environmental variation can lead to mode coupling. These include a sloping bottom, bottom and surface roughness, the presence of biomass, and currents

or other disturbances in the water column. One particularly dramatic example of a water column distubance is the phenomenon of internal waves. These waves form in areas with strong density gradients and can generate large displacements in the layers of the water column which could result in significant mode coupling.

1.2 Internal Waves

In the open ocean, the internal wave field can best be described as a stochastic phenomenon with broadband frequency and wavenumber distribution [2]. In shallow coastal zones, however, internal waves can exist as solitons. Figure 1-2 shows an example of a packet of internal solitary waves recorded using a 200 kHz sonar in Massachusetts Bay (from [3] pp. 315). The sonar was mounted to a research vessel

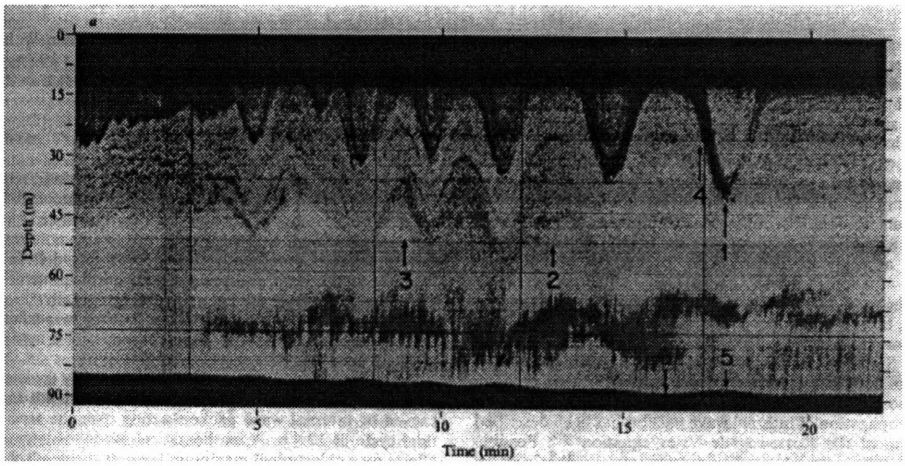

Figure 1-2: Internal Wave Packet in Massachusetts Bay

which then steamed through an area of internal wave activity. Figure 1-2 shows the sonar return from plankton and fine scale temperature and density variations in the water column as a function of time (position) on the horizontal axis and depth on the vertical axis. Internal waves displacing the horizontal layer structure by up to 20 meters are distinctly visible.

Tidal flow over significant bathymetry features such as shelves, banks and canyons

can generate these solitons at very regular and predictable times and frequencies. These solitons have been observed in coastal zones virtually worldwide from their expression on currents [4], modulation of surface gravity waves [5, 6], high frequency acoustic profiling [3, 7], and temperature measurements [4, 3].

Acoustic observations internal waves have been primarily limited to stochastic studies of the travel time perturbations in the stochastic, open ocean environment. For example, Essen et. al. [8] did a study with a single source and receiver correlating the observed variation of arrival phase and amplitude presumably due to internal waves with data from a current meter. Zhou, Zhang, and Rogers [9] made a limited investigation into the mode coupling effects of solitary internal wave packets in 1991. Their research used acoustic propagation simulations based on the parabolic equation and a model of internal wave disturbances to try to match anaomalous transmission loss data from a previous long range transmission experiment in the Sulu Sea. In this research, they also described some of the basic mode coupling behaviours caused by internal wave packets such as wavenumber and packet length resonance. This thesis summarizes the author's research the mode coupling behaviour caused by packets of solitary internal waves and whether we could use our single mode transmission system to observe and parameterize the wave packets.

1.3 Organization

In Chapter 2 we describe the models of both our coastal ocean environment and the form of solitary internal wave packets. We also describe the two types of simulations we used for our research.

In Chapter 3 we look at the theory of simple mode coupling behaviours and present some simulations to demonstrate them. These include the wavenumber and packet length resonance resonance effects mentioned previously. In this chapter much of the theory is based on similar mode coupling behaviour in the propagation of electromagnetic waves in optical fibres and other dielectric waveguides. This has been studied extensively by Marcuse [10], among others, and is helpful in extending

the theory introduced by Zhou, Zhang, and Rogers.

In Chapter 4 we proceed using more accurate descriptions of the internal waves we are likely to see in the region chosen for our test. We extend our observation of wavenumber and packet length resonance behaviour into cases which cause breakdowns in the simple behaviour described in Chapter 2. We also present a sensitivity analysis of the mode coupling to changes in the internal wave shapes and parameters to check whether an inverse problem is possible.

Finally in Chapter 5 we summarize the implications of the research and suggest directions for future work.

This page left blank.

Chapter 2

Models

In this chapter we describe the models used to describe both acoustic and internal wave propagation. We try to justify the accuracy and level of sophistication of these models with a view to the phenomana under investigation and the effort involved. We also present an overview of the numerical tools used throughout the research.

2.1 Environment

We have based the research for this thesis on a two layer model of the water column, as shown in Figure 2-1 and Table 2.1. Two layers of homogeneous water occupy the

c_1	c_2	h_1	h_2	D	c_b	ρ_b	B
1522 m/s	1494 m/s	10 m	30 m	50 m	1673.3 m/s	2 g/cm^3	200 m

Table 2.1: Environmental Parameters

top and the bottom of the water column with sound speed c_1 and c_2 respectively. The water between the two layers has a linear sound speed profile with endpoints matching the sound speed at the inferfaces to the upper and lower layers. A homogenous sediment layer extends from the bottom depth D to a pressure-release half-space beginning at the basement depth B. Our choices of sound speeds c_1 and c_2 and the interface depths $h1$, $h2$, and D are averages from sound speed and bathymetry data

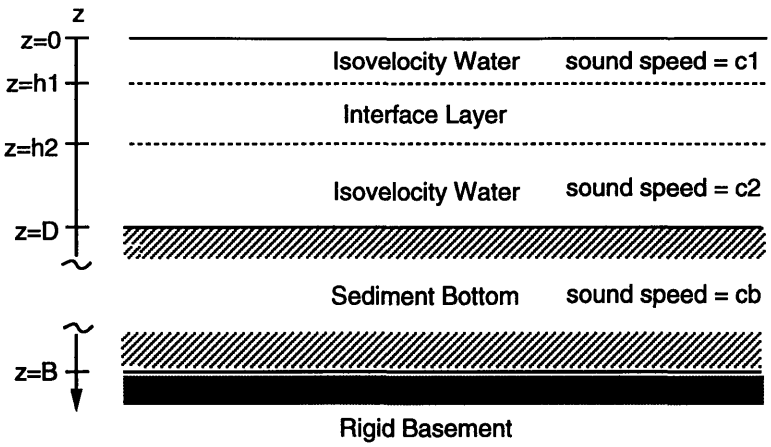

Figure 2-1: Unperturbed Environmental Model

taken in August 1993 in an area of Vineyard Sound which showed evidence of solitary internal wave activity. The bottom parameters c_b and ρ_b and the basement depth B are taken from an oceanographic database in the same area.

2.1.1 Acoustics

Figure 2-2 shows a modal decomposition of the unperturbed environmental model. The first nine modes are propagating modes in the water column. The higher order modes are leaky modes and carry most of their energy in the bottom. We will primarily be concerned with the propagating modes, as we have no way of making pressure measurements in the bottom sediment layer. In fact, the leaky modes are attenuated quickly due to absorption in the bottom sediments, where the attenuation coefficient $\beta = 1.70\text{dB/m/kHz}$.

2.1.2 Hydrodynamics of Internal Waves

In the hydrodynamic model the density gradient is the feature which allows the internal waves to form and propagate, so that density cannot be considered as constant

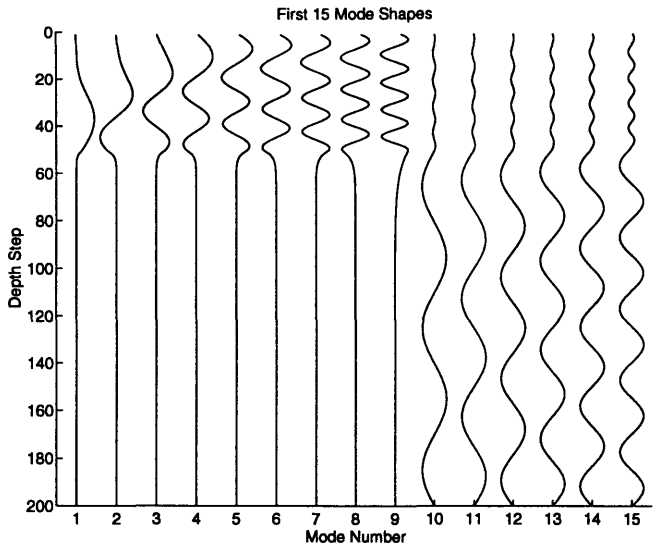

Figure 2-2: Normal Modes of the Unpurturbed Environmental Model

through the water column as it is while generating the acoustic mode shapes. We have sound speed and temperature data for the area in which we will be carrying out our experiments but we do not have any salinity data. Therefore in our model we based the density gradient on measured changes in temperature.

One can approximate the internal wave displacement field η by a function of the form [5],

$$\eta(x,z,t) = A(x,t)\phi(z)$$

$\phi(z)$ is dimensionless with maximum value normalized to unity so that $A(x,t)$ represents the maximum vertical displacement η. Under certain conditions, perturbation methods can be applied to find simplified, first order solutions for ϕ and A.

It turns out that ϕ can be approximated by the eigenvalue equation,

$$\frac{\partial^2\phi}{\partial z^2} + \frac{N^2(z)}{C_0^2}\phi = 0 \tag{2.1}$$

with boundary conditions,

$$\phi(0) = \phi(D) = 0$$

where $N(z)$ is the buoyancy frequency profile,

$$N^2(z) \equiv -\frac{g}{\rho_0}\frac{d\rho}{dz},$$

and C_0 is the phase speed of long linear internal waves.

Figure 2-3 shows the buoyancy frequency profile $N(z)$ and the first few modes of the solution of Equation 2.1 for our environmental model. Halpern's observations of

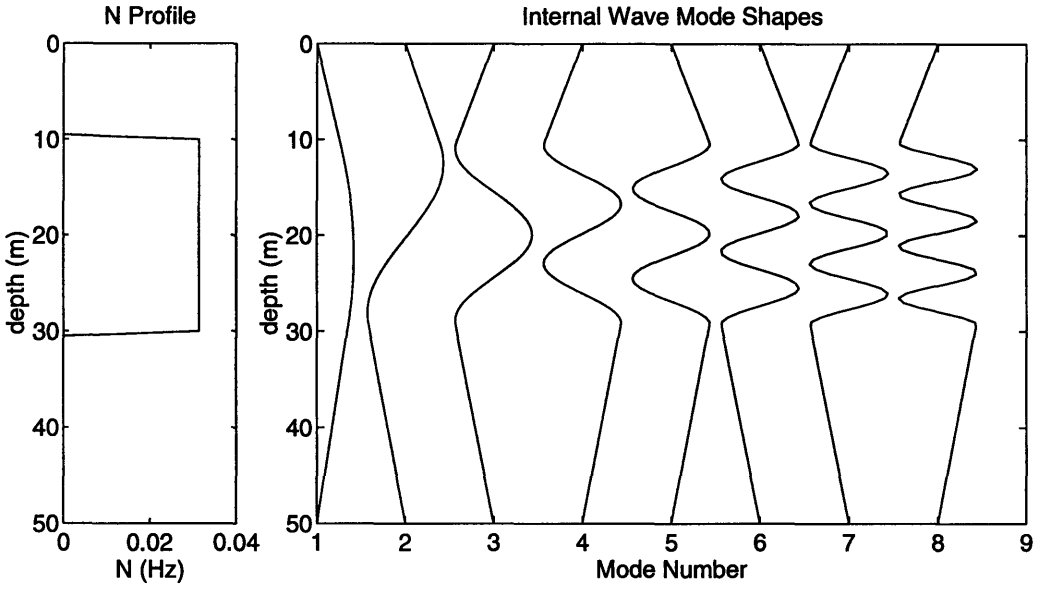

Figure 2-3: Buoyancy Profile and Internal Wave Modes

internal waves in Massachusetts Bay [4] showed a measured vertical displacement $\phi(z)$ which agreed within 10% with the calculated displacement for the first eigenfunction. Therefore many authors [9, 5, 11] consider only the first mode in an approximation of the vertical structure $\phi(z)$. We will take the approximation a step farther and eliminate the vertical structure $\phi(z)$ altogether from our internal wave model.

A second look at the mode structure in Figure 2-3, keeping our environmental model in mind, shows that this may not be a bad approximation. Any displacement occuring above $h_1 = 10$ meters or below $h2 = 30$ meters has no physical effect on

the environmental model — it merely displaces water with the same sound speed characteristics. Thus we need only to be concerned with the vertical displacement inside the interval $[h_1, h_2]$. For mode one inside this interval $\phi(z)$ ranges from about 0.6 at 10 meters to 0.8 at 30 meters with the maximum of 1.0 ocurring near 20 meters. We have chosen to use $\phi(z) = 1.0$ throughout the interval, in effect displacing the interface depths h_1 and h_2 in the unperturbed model by $A(x,t)$ and eliminating the vertical structure from the model.

A zeroth order perturbation solution [5] for $A(x,t)$ leads to a form of the Korteweg-de Vries equation [12],

$$A_t + C_0 A_x + \alpha A A_x + \gamma A_{xxx} = 0$$

which has a soliton solution,

$$A(x,t) = a\,\mathrm{sech}^2\left(\frac{x - ct}{L}\right) \tag{2.2}$$

The amplitude a and half-length L from this expression are related through the equation,

$$aL^2 = \frac{4}{3}\frac{(H_1 H_2)^2}{H_2 - H_1}$$

where $H1$ is the distance from the surface to the middle of the interface layer and $H2$ is the distance from the middle of the interface layer to the bottom (for our model: $H1 = 20$ m, $H2 = 30$ m).

We have presented a solution for A as a sech^2 function. However, we know that these solitons are generated in groups [3, 4, 5, 6, 7] and that they are non-linear so that a group of sech^2 waves cannot simply be added together. We decided to represent $A(x,t)$ as a sin function with parameters determined from the relations for the soliton solutions above. This approach has been used with some success in the past [9, 11]. In fact, as we show in Chapter 4, the exact shape of A does not affect the type of mode coupling phenomena which occur but does determine when and if it will occur. Figure 2-4 shows a typical example of the type of environmental disturbance studied

throughout this thesis. A periodic perturbation to the interface depths h_1 and h_2

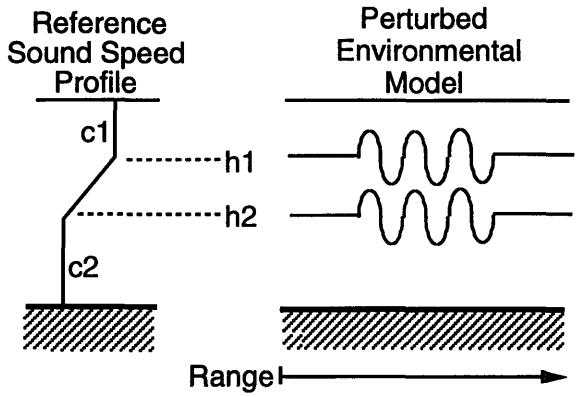

Figure 2-4: Typical Waveguide Perturbation

begins at some intitial range r_i and continues for an integral number of periods.

2.2 Numerical Tools

We used two different numerical methods for simulating the acoustic propagation throught the perturbed model and evaluating the resulting mode coupling. In one case, we used the perturbed environmental parameters in an acoustic propagation code capable of dealing with a range dependent environment. In the second, we implemented a numerical solution to a system of coupled differential equations derived by inserting the environmental parameters into the equations for acoustic propagation.

We used FEPE, an acoustic propagation code based on a parabolic equation method and written by Michael Collins [13]. This is a well used and well tested piece of code and includes a routine for solving the normal mode eigenfunctions and eigenvalues which we used to calculate the unperturbed mode shapes. We used a simple projection onto the eigenvectors to decompose the output field of the PE code and calculate the mode coefficients.

We derive the mode coupling equations used in our second method in detail in Appendix A and present the reuslts in Chapter 3. They are based on the sound

speed profile perturbation $\delta c(z)$ caused by the displacement of the unperturbed profile by the internal waves. There is another approach based on the perturbations in the eigenvalues and eigenfunctions of the resulting local modes. We selected the first method because it gives results more clearly in terms of the displacement field parameterization we used for our internal wave disturbance.

This page left blank.

Chapter 3

Mode Coupling Effects

To begin our theoretical analysis we must first choose or develop a mode coupling formulation. The first applications of normal modes to range dependent environments were developed separately by Pierce [14] and Milder [15]. Their formulation uses local modes and their spatial derivatives to develop a system of coupled ordinary differential equations.

This formulation has been applied to and developed for various types of range dependence in the environment. These include stepwise bathymetry changes by Evans [16], constant slope bottoms by Graves et. al. [17] and Jensen and Tindle et. al. [18, 19], range dependent velocity profiles by Chwieroth et. al [20] and Desaubies et. al. [21], and more general bathymetry and bottom property changes by McDaniel [22, 23].

An alternate formulation using the same approximations but based on a reference sound speed profile and perturbations to that profile has been used by Kohler and Papanicolaou [24] to describe propagation in a randomly inhomogeneous ocean and specifically applied to random, open ocean internal waves by Dozier and Tappert [25]. We prefer this formulation because it gives results directly in terms of the parameters of our internal wave distubances, rather than indirectly through their effect on the eigenvalues and eigenfunctions of the local modes.

Appendix A steps through a detailed theoretic development leading to the following system of coupled mode equations used by Kohler and Papanicolaou [24] and

Dozier and Tappert [25],

$$\frac{\partial \psi_m}{\partial r}(r) = -i \sum_n \psi_m(r) R_{mn}(r) e^{ik_{mn}r}, \tag{3.1}$$

with

$$R_{mn}(r) = \frac{2}{\sqrt{k_m k_n}} \int dz \frac{\omega^2}{c_o^2(z)} \frac{\delta c(r,z)}{c_o(z)} Z_n(z) Z_m(z),$$

$$k_{mn} = k_n - k_m.$$

where $Z_m(z)$ are the mode functions for the unperturbed environment with horizontal wavenumbers k_m, $c_o(z)$ is the unperturbed sound speed profile, and $\delta c(r,z)$ is the perturbation to the sound speed profile caused by the vertical displacement of the water column by the travelling internal waves. The pressure field may be expressed in terms of these mode coefficients as,

$$P(r,z) = \frac{1}{\sqrt{r}} \sum_n \psi_n(r) e^{ik_n r} Z_n(z) \tag{3.2}$$

Let's examine the effect of a typical internal wave displacement on the coupling coefficient $R_{nm}(r)$ given our model environment. For small internal wave amplitudes a, we can approximate the integral for R_{nm} by replacing $\delta c(r,z)$ by its maximum value in depth $\delta c_{max}(r)$ and integrate over the (constant) interval $[h_1, h_2]$. Then $\delta c_{max}(r)$ comes outside the integral and we can replace $c_o(z)$ by an average value $\bar{c_o} = (c_1 + c_2)/2$ and remove that from the integral as well. We are left with,

$$R_{mn}(r) = \frac{1}{\sqrt{k_m k_n}} \frac{\omega^2}{\bar{c_o}^2} \frac{\delta c_{max}(r)}{\bar{c_o}} \tilde{Z}_{nm}, \tag{3.3}$$

where,

$$\tilde{Z}_{nm} = \int_{h_1}^{h_2} dz Z_n(z) Z_m(z)$$

Since ω and $\bar{c_o}$ are independent of the mode numbers n and m, we see that there are two factors which determine the size of the mode coupling coefficient: $\delta c_{max}(r)$, which is determined by the internal wave diplacement $\eta(r)$, and the term $\tilde{Z}_{nm}$ based on the correlation of the two mode eigenfunctions over the interval $[h_1, h_2]$. The term

$\sqrt{k_m k_n}$ in the denominator doesn't change appreciably over the range of eigenvalues k_n of the propagating modes.

Though these approximations break down in some cases (see Chapter 4), especially for large internal wave amplitudes, they enable us to get some insight into two of the most prominent features of the resulting mode coupling: wavenumber resonance and packet length resonance.

3.1 Wavenumber Resonance

Wavenumber resonance describes the phenomenon whereby significant mode coupling occurs only if the length structure of the disturbance matches the length scale of the wavenumber difference between a pair of modes. This can be illustrated by a simple example based on the mode coupling equations introduced in the previous section.

If we assume that all the energy is initially in a single mode p then we have the initial conditions $\psi_p(0) = 1, \psi_n(0) = 0$ for $n = 1, \ldots, N$ and $n \neq p$. If we further assume that we are interested in the solution in a limited range where the mode coefficients do not change appreciably, then the equations decouple and we can obtain solutions by straightforward integration,

$$\psi_n(r) = -i\psi_p(0) \int_0^r dr' R_{np}(r') e^{ik_{np}r'}$$

Now we further assume that the range variation in $\delta c/\bar{c_o}$ is described by the function $f(r)$ so that the coupling coefficients may be written as,

$$R_{nm}(r) = \hat{R}_{nm} f(r)$$

In fact, as we showed in Equation 3.3, for small internal wave amplitudes the function $f(r)$ is simply the internal wave displacement field $\eta(r)$. Now we can see that the fourier transform $F(k)$ of $f(r)$ appears in the solutions,

$$\psi_n(r) = -i\psi_p(0)\hat{R}_{np} \int_0^r dr' f(r') e^{ik_{np}r'} = -i\psi_p(0)\hat{R}_{np} L^{1/2} F(k_{np})$$

where

$$F(k) = L^{-1/2} \int_0^r dr' f(r') e^{ikr'}.$$

We see that coupling occurs only in the case that the fourier transform of the disturbace $F(k)$ has appreciable amplitude at wavenumber difference frequency k_{nm}. Figures 3-1 and 3-2 show this effect for a sinusoidal internal wave disturbance,

$$f(r) = \begin{cases} \sin(k_{int} r), & r_i < r < r_i + 15\lambda_{int} \\ 0, & \text{otherwise} \end{cases}$$

with a packet length of 15 wavelengths. The fraction of the total acoustic energy

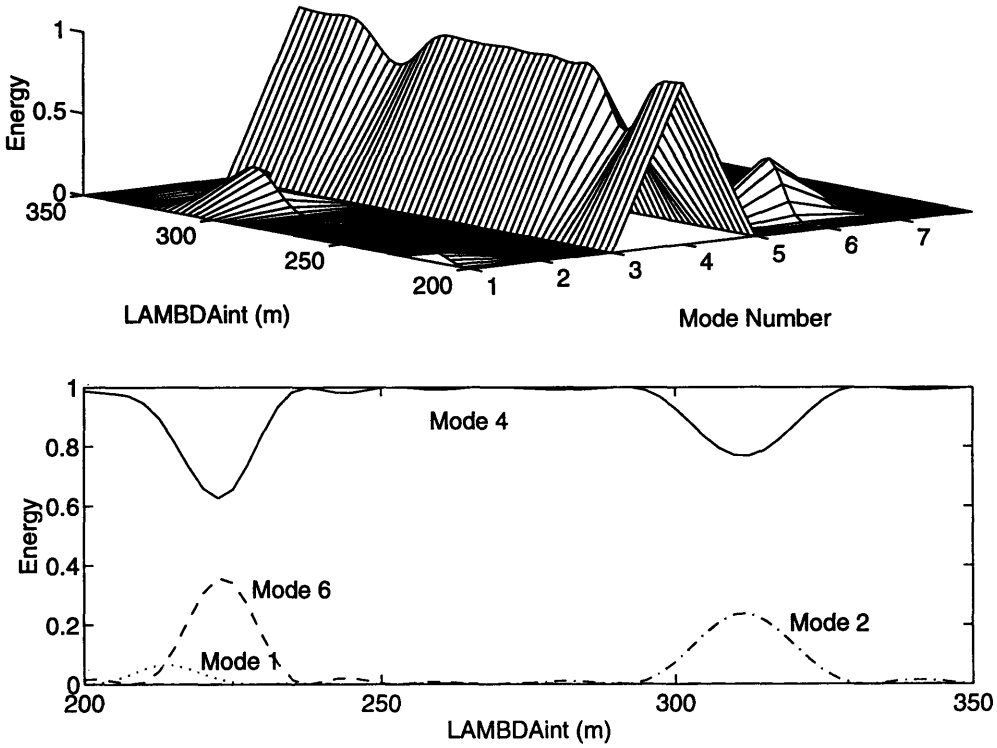

Figure 3-1: Wavenumber Resonance Effect: Solution of Coupled Mode Equations

in each mode after propagating through the 15 soliton packet of the type shown in Figure 2-4 is shown as a function of the soliton wavelength λ_{int}. We generated the data for Figure 3-1 using a numeric solution of our coupled mode equations. We

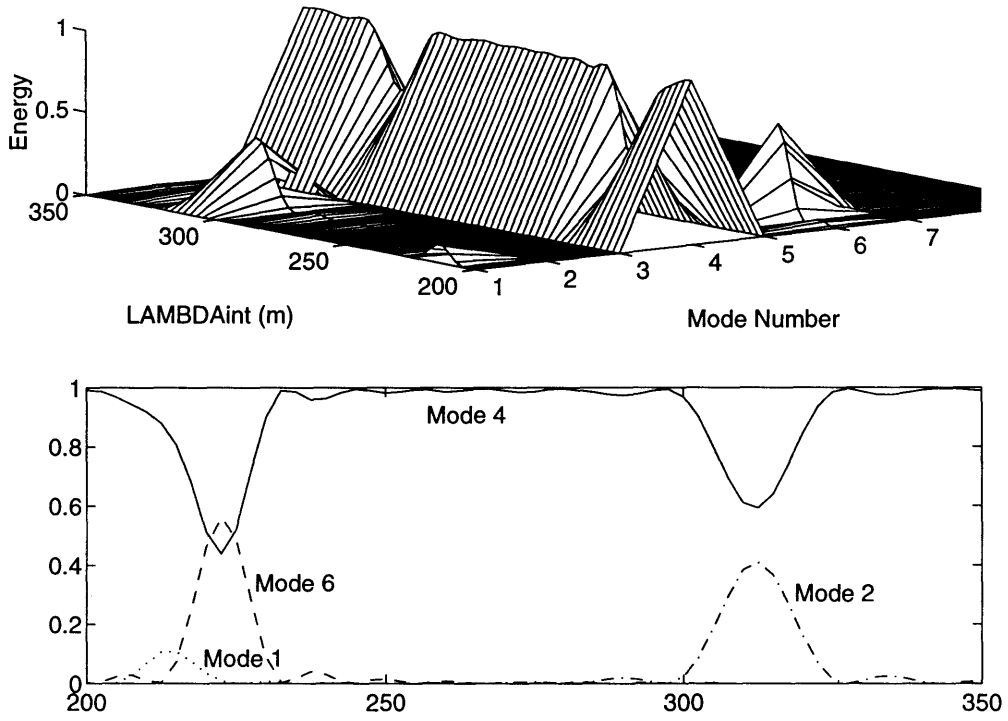

Figure 3-2: Wavenumber Resonance Effect: FEPE Simulation

verified the accuracy of the coupled mode model by running FEPE on the same environmental disturbance. Figure 3-2 shows that result.

We see that the acoustic energy, which is initially all in mode 4, shows significant coupling to other modes only near a few specific wavelengths. Comparing the observed wavelengths from the figure to those in Table 3.1 we see that coupling to other modes occurs only when the spatial frequency of the internal waves k_{int} matches one of the mode difference wavenumbers k_{mn}. Coupling occurs from mode 4 to modes 1 and 6

m \ n	1	2	3	4	5	6	7	8	9
1	•	-686.7	-326.6	-214.4	-151.2	-109.3	-81.6	-62.9	-49.8
2	686.7	•	-622.7	-311.7	-193.9	-129.9	-92.6	-69.2	-53.7
3	326.6	622.7	•	-624.0	-281.6	-164.2	-108.8	-77.9	-58.7
4	214.4	311.7	624.0	•	-513.3	-222.8	-131.8	-89.0	-64.8
5	151.2	193.9	281.6	513.3	•	-393.7	-177.3	-107.6	-74.2
6	109.3	129.9	164.2	222.8	393.7	•	-322.7	-148.1	-91.4
7	81.6	92.6	108.8	131.8	177.3	322.7	•	-273.7	-127.6
8	62.9	69.2	77.9	89.0	107.6	148.1	273.7	•	-239.1
9	49.8	53.7	58.7	64.8	74.2	91.4	127.6	239.1	•

Table 3.1: Wavenumber Difference Wavelengths $\lambda_{nm} = 2\pi/k_{mn}$ (m)

for λ_{int} near λ_{41} and λ_{46} and from mode 4 to mode 2 for λ_{int} near λ_{42}. The difference in the amount of coupling is a function of the number of solitons in the packet, or the packet length. We discuss this relationship in the next section.

3.2 Packet Length Resonance

The mode coupling experienced as acoustic waves propagate through a packet of internal solitary waves exhibits two separate resonance effects. The first is a wavenumber resonance in which considerable mode coupling occurs only for internal waves with characteristic wavenumbers k_{int} which are close to the wavenumber difference k_{nm} between any two modes n and m. The second is a packet length resonance which causes the coupling to vary periodically with the packet length P_L with some spatial

frequency K_P. We can gain some insights into this behaviour through an examination of the coupled mode equations A.9 from the previous section.

Assume we have a system where we concern ourselves with the coupling between only two modes p and q. For this to be true the coupling between these two modes must dominate the coupling from general scattering over the lengths of interest. In their research Zhou, Zhang, and Rogers [9] showed that this is the case for distances up to 30 km. Continuing with the analysis, from A.9 we have the system,

$$\frac{\partial \psi_p}{\partial r} = -iR_{pp}\psi_p - iR_{pq}e^{ik_{pq}r}\psi_q,$$

$$\frac{\partial \psi_q}{\partial r} = -iR_{qp}e^{ik_{qp}r}\psi_p - iR_{qq}\psi_q.$$

Now we assume that the variation in $\delta c(r,z)$ goes as $sin(k_{int}r)$. Substitute $R_{nm}(r) = \hat{R}_{nm}(e^{ik_{int}r} - e^{-ik_{int}r})/i2$ to obtain,

$$\frac{\partial \psi_p}{\partial r} = -\frac{\hat{R}_{pp}}{2}\left[e^{ik_{int}r} - e^{-ik_{int}r}\right]\psi_p - \frac{\hat{R}_{pq}}{2}\left[e^{i(k_{int}+k_{pq})r} - e^{i(k_{int}-k_{pq})r}\right]\psi_q,$$

$$\frac{\partial \psi_q}{\partial r} = -\frac{\hat{R}_{qp}}{2}\left[e^{i(k_{int}+k_{qp})r} - e^{i(k_{int}-k_{qp})r}\right]\psi_p - \frac{\hat{R}_{qq}}{2}\left[e^{ik_{int}r} - e^{-ik_{int}r}\right]\psi_q.$$

We see that there are three scales of variation on the right hand sides of these equations: $(k_{int} - k_{pq}) \approx 0$, $k_{int} \approx k_{pq}$ and $(k_{int} + k_{pq}) \approx 2k_{int}$. If we keep only the slowly varying $k_{int} - k_{pq}$ term we then get the system,

$$\frac{\partial \psi_p}{\partial r} \approx \frac{\hat{R}_{pq}}{2}\psi_q,$$

$$\frac{\partial \psi_q}{\partial r} \approx \frac{\hat{R}_{qp}}{2}\psi_p.$$

Marcuse [10] accomplishes this step by performing a spatial averaging over the scale k_{int}^{-1} thus eliminating all remaining sinusoidally varying terms. The justification is that the mode amplitudes $\psi_{p,q}$ do not vary substantially over this short k_{int}^{-1} length scale. The resulting expression is in fact a poor approximation of $\partial\psi_{p,q}/\partial r$ but because this is a two-scale process, the solutions $\psi_{p,q}$ of the spatially averaged equations predict

the long-scale behavior of the resulting coupling very well.

Combining the two equations we find,

$$\frac{\partial^2 \psi_{p,q}}{\partial r^2} = \frac{\hat{R}_{pq}}{2}\frac{\hat{R}_{qp}}{2}\psi_{p,q} = \frac{\hat{R}_{pq}^2}{4}\psi_{p,q},$$

which has the solutions,

$$\psi_{p,q} = \sin\frac{\hat{R}_{pq}}{2}r, \cos\frac{\hat{R}_{pq}}{2}r.$$

If we initially have $\psi_p = 1, \psi_q = 0$ then the solutions become $\psi_p = \cos\hat{R}_{pq}r$, $\psi_q = \sin\hat{R}_{pq}r$. The acoustic energy travels from mode p to mode q and back again as the sound field propagates through the packet. We also see that the spatial frequency of this variation K_L is proportional to the mode coupling coefficient $\hat{R}_{pq}$. Looking at the structure of $\hat{R}_{pq}$ we can make some predictions about this behaviour.

Again using our sinusoidally varying internal wave model, then from Equation 3.3 we have,

$$\hat{R}_{mn} = \frac{1}{\sqrt{k_m k_n}}\frac{\omega^2}{\bar{c}_o^2}\frac{\delta c_{max}}{\bar{c}_o}\tilde{Z}_{nm}$$

There are two varying terms which affect the magnitude of $\hat{R}_{pq}$: the amplitude of the internal wave displacement determines the magnitude of δc and the mode correlation factors $\tilde{Z}_{nm}$ which we have calculated in Table 3.2. We can use these values to predict the packet length resonance frequency K_L. Thus we would expect that an increase in either of these two factors would cause a corresponding increase in the wavenumber K_L and the mode coupling would vary more quickly with packet length. This variation is demonstrated below.

Figure 3-3 shows the effect of packet length resonance very clearly. Data generated by solving the coupled mode equations is labelled CME and data generated by FEPE is labelled FEPE. The plot in the upper left shows coupling from mode 4 to mode 2 and back into mode 4 as the acoustic energy propagates through the sinusoidal internal wave disturbance. All the other modes contain very little energy over all ranges and are barely noticeable above the Packet Length axis at the bottom of the plot. Since the modes travel independently, without coupling, in the unperturbed waveguide, we

m \ n	1	2	3	4	5	6	7	8	9
1	0.1717	0.2775	0.0893	0.1397	0.0367	0.0711	0.0776	0.0171	0.0693
2	0.2775	0.5093	0.3092	0.1817	0.0528	0.0903	0.0698	0.0445	0.0767
3	0.0893	0.3092	0.5453	0.1655	0.2585	0.1477	0.0288	0.0140	0.0229
4	0.1397	0.1817	0.1655	0.4336	0.0069	0.3256	0.1401	0.0236	0.0090
5	0.0367	0.0528	0.2585	0.0069	0.3418	0.0574	0.2925	0.1389	0.0838
6	0.0711	0.0903	0.1477	0.3256	0.0574	0.3626	0.1095	0.2049	0.1412
7	0.0776	0.0698	0.0288	0.1401	0.2925	0.1095	0.4337	0.1241	0.2331
8	0.0171	0.0445	0.0140	0.0236	0.1389	0.2049	0.1241	0.3819	0.1303
9	0.0693	0.0767	0.0229	0.0090	0.0838	0.1412	0.2331	0.1303	0.3602

Table 3.2: Packet Length Resonance Factors

can interperet the mode coefficients at any point along the packet length axis as the coupling which would result from a sinusoidally shaped wave packet of that length located anywhere between the acoustic source and receiver arrays.

The analysis presented earlier predicted a packet length resonance frequency of $K_L = \hat{R}_{pq}/2$. For mode $p = 4$ and $q = 2$ this corresponds to $\lambda_{42}/2 = 29.8$ km ≈ 96 packets, closely matching the period shown on the upper left plot.

The plots on the right show the same situation but with the amplitude of the internal wave disturbance doubled. Then Equation 3.3 predicts a corresponding doubling of K_L or halving of λ_L as shown in the right hand plots.

The other factor affecting $\hat{R}_{mn}$ is the mode shape integral factor $\tilde{Z}_{mn}$. Figure 3-4 shows this effect on the packet length resonance wavelength for coupling from mode 4 to mode 6. DFrom the data in Table 3.2 we see that the mode coupling factor $\tilde{Z}_{46} \approx 1.75\tilde{Z}_{42}$ which should give a packet length resonance wavelength $\lambda_{L46} \approx \lambda_{L42} \approx 17.0$ km ≈ 76 packets, agreeing very well with that shown by the left hand plots.

For the plots on the right the amplitude of the internal wave disturbance was again doubled. This is reflected in the shortened resonance wavelengths shown in the figure. Also shown is the increasing effect of coupling from mode 4 to mode 1, which the wavenumber resonance analysis of the previous section predicted would also exist for this interference wavelength.

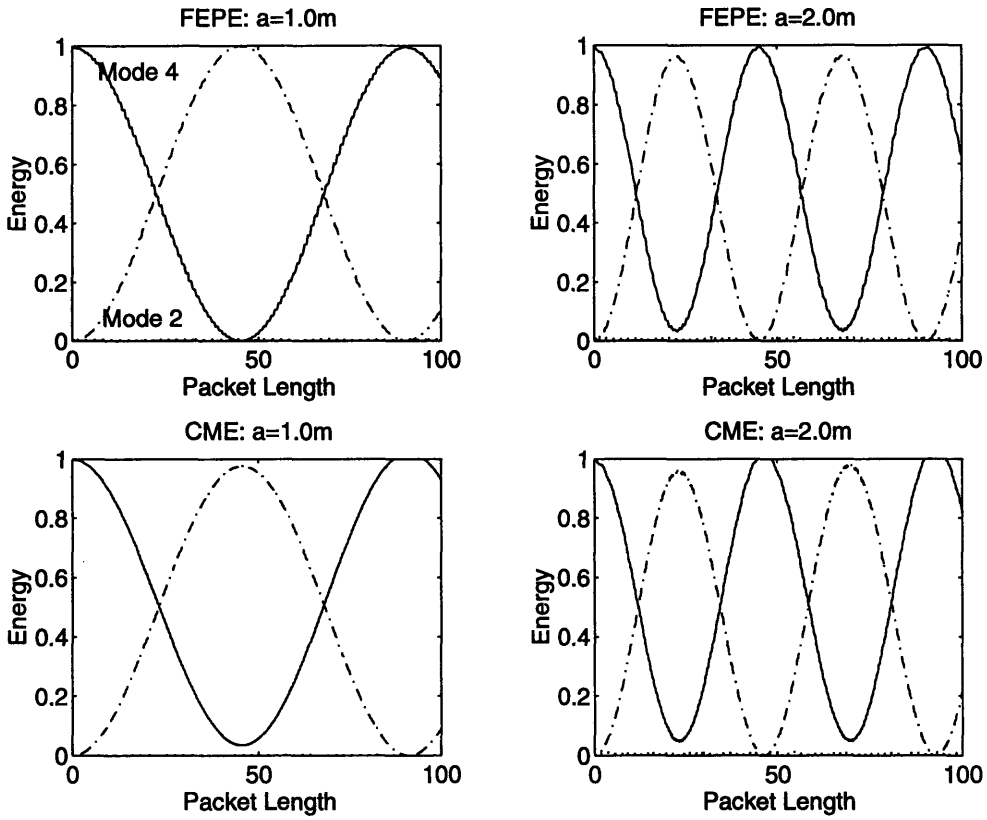

Figure 3-3: Packet Length Resonance Effect: $\lambda_{int} = 312.0$ meters

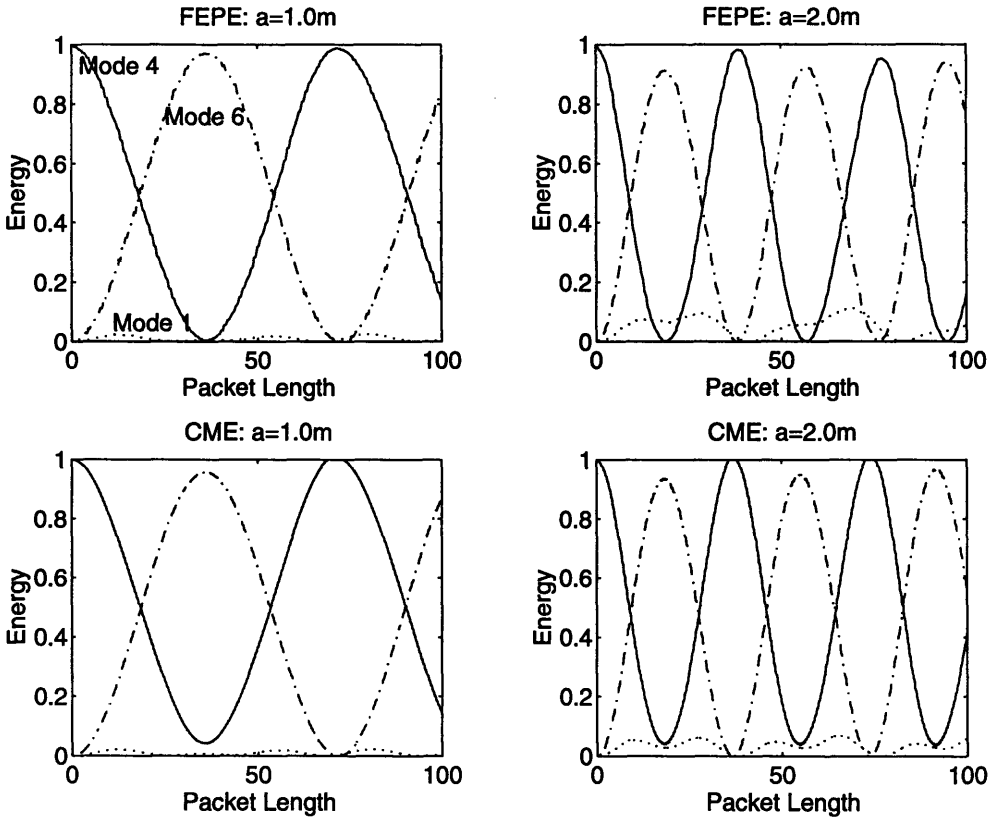

Figure 3-4: Packet Length Resonance Effect: $\lambda_{int} = 222.3$ meters.

This page left blank.

Chapter 4

Simulations and Discussion

Now that we have some idea of the causes of mode coupling for internal wave disturbances, we would like to generate some more realistic models of the types of internal wave disturbances we could actually see in the area where we will be experimenting. This includes more realistic wave shapes with displacement of the water column downwards only and a shape which more closely approximates the sech^2 function which is a solution to the internal wave equation. We try to extend the simplified analysis of the previous section to these more realistic wave shapes and amplitudes. We show examples of how the simple wavenumber and packet length resonance behaviors we examined in Chapter 3 apply to these more realistic waveforms. We also show cases where these predictions fail and explain some of the causes of this failure. Finally we present a simulation of an experimental configuration and show the features of the internal waves which can be deduced from the observed mode coupling.

4.1 Improved Internal Wave Models

Figure 1-2 showed the shape of an internal wave packet observed in Massachusetts Bay and recorded by a 200 kHz sonar. Several features of this wave packet differ from the models we used in Chapter 3. These include displacement of the water column down from the top interface only, the not quite sinusoidal shape of the waves themselves, and the irregular spacing and wave amplitudes and widths. We now introduce a few

improved models which take these features into account.

We used three different internal wave models for the simulations in this chapter. Figure 4-1 shows the displacement functions applied using each of the three models. In all cases the wave displacement is strictly positive. For our first improved model

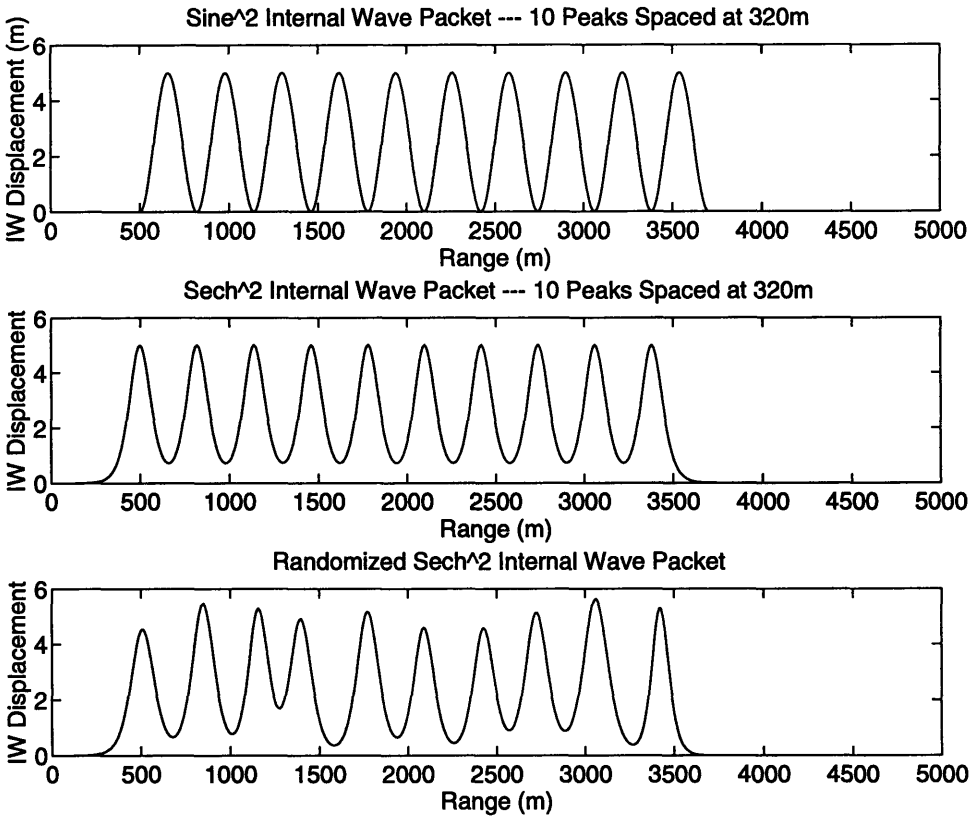

Figure 4-1: Improved Internal Wave Displacement Functions — $\lambda_{int} = 320$m

we kept the same wave shape but obtained one-sided displacement by changing the sin function to a $\sin^2$. Next we modified the shape of the individual wave peaks to match the hyperbolic secant function as described in Equation 2.2. We discuss the results for these $\sin^2$ and sech^2 models in Sections 4.2 through 4.4. Finally we randomized the spacing, amplitude, and width of the waves in the packet to better simulate conditions in the real ocean, as we discuss in Section 4.5.

4.2 Predictable Behavior

From our discussions of wavenumber and packet length resonance in Chapter 3 we can predict the wavelengths where large amplitude waves cause significant coupling and the spatial frequency of the packet length resonance associated with this coupling. We present a small set of predicted coupling pairs and wavelengths, and their packet length resonance periods λ_{PL} in Table 4.1.

Mode Pair	Difference Wavelength (m)	λ_{PL} (km): ($\eta = 5.0$ m)	$R_{nm}(\eta = 7.5$ m)
$2 \leftrightarrow 4$	311.7	4.8	3.3
$3 \leftrightarrow 5$	281.6	3.1	2.1
$4 \leftrightarrow 6$	222.8	3.5	2.6
$3 \leftrightarrow 6$	164.2	n/a	n/a

Table 4.1: Predicted Packet Length Resonance Wavelengths

We tested these predictions using FEPE to simulate the propagation of single mode starting fields through 5km of ocean containing a single packet of ten internal wave peaks with wave height $\eta = 5.0$m and 7.5m and various wave spacings λ_{int} with the leading edge of the packet located at a range of 500 meters. Figures 4-2 though 4-4 show the simulation results for the first three coupling pairs from Table 4.1.

The first thing we notice is that strong coupling does occur between the predicted mode pairs. The energy is transferred back and forth between modes in the same coupled oscillator like fashion that we observed with the small amplitude sinusoidal waves in Chapter 3. The increased displacement amplitude results in much shorter packet length resonance lengths λ_{PL} and distortion to the coupling curves.

The observed packet length resonance lengths λ_{PL}, though the same order as those predicted in Table 4.1, do not match nearly as well as the small amplitude examples from Chapter 3. Furthermore, as Figure 4-5 shows, the $3 \leftrightarrow 6$ mode pair does not experience significant coupling even though its difference frequency $\lambda_{36} = 164.2$ meters is very close to the internal wave spacing length $\lambda_{int} = 160$ meters. In the next section we investigate the causes of this anomalous coupling behavior.

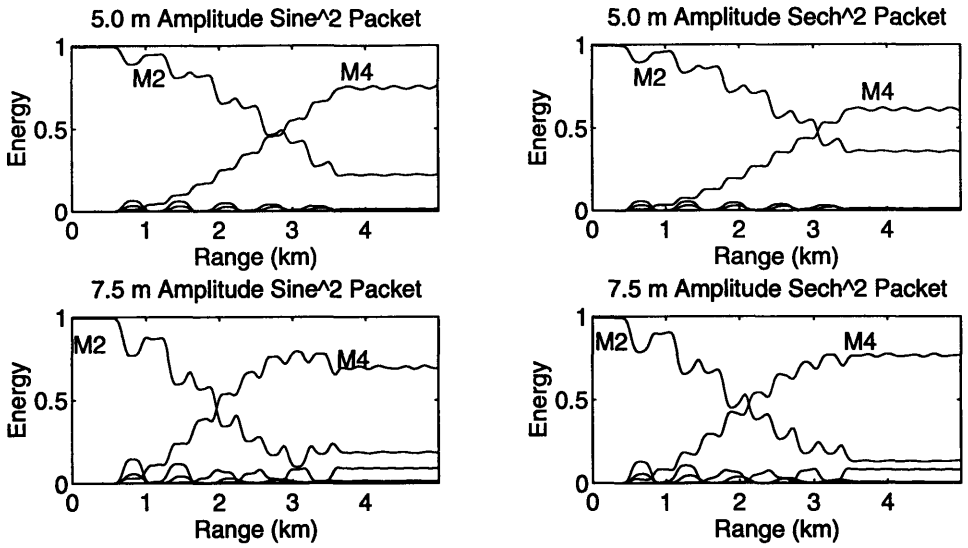

Figure 4-2: Coupling from High Amplitude Internal Waves, $\lambda_{int} = 320$ m

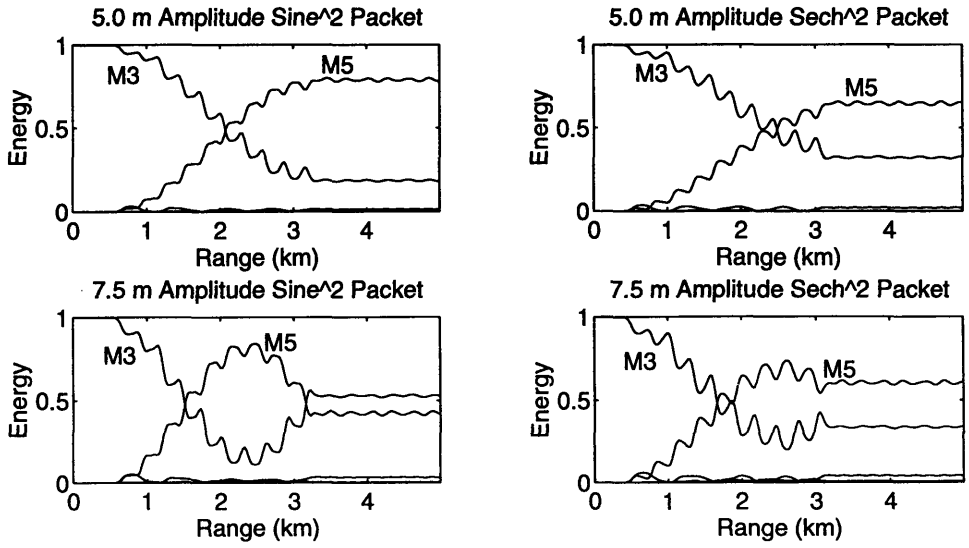

Figure 4-3: Coupling from High Amplitude Internal Waves, $\lambda_{int} = 280$ m

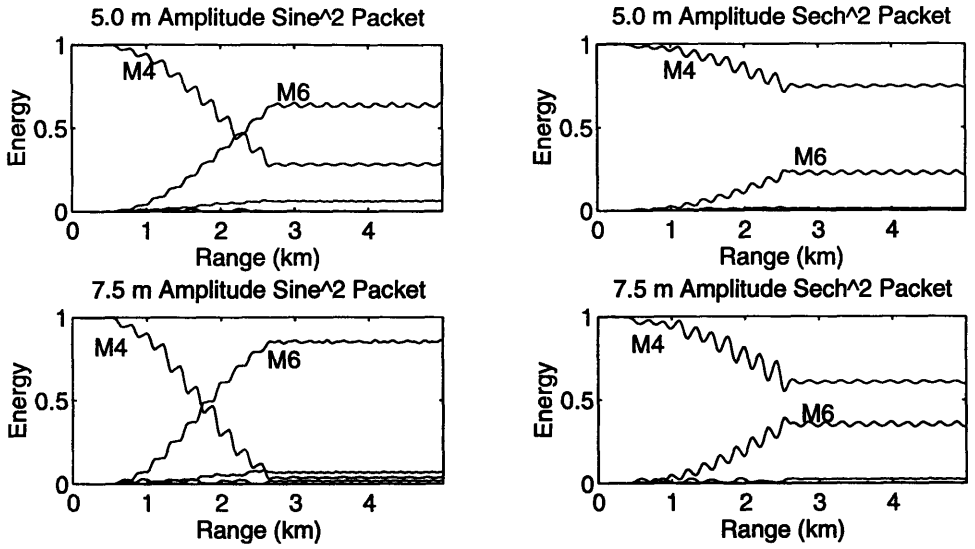

Figure 4-4: Coupling from High Amplitude Internal Waves, $\lambda_{int} = 220$ m

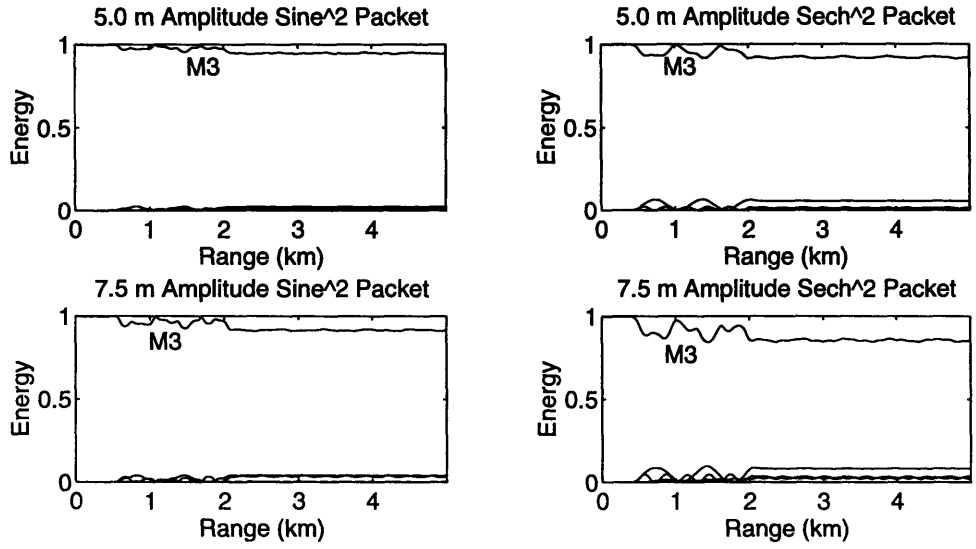

Figure 4-5: Coupling from High Amplitude Internal Waves, $\lambda_{int} = 160$ m

4.3 Breakdown of Wavenumber Resonance Predictions

In Section 3.1, we showed that under certain conditions the Fourier Transform of the internal wave displacement function at the mode difference frequencies determines whether coupling will occur between the respective mode pairs. Figure 4-5 from the previous section showed an example where this Fourier Transform analysis predicts coupling between the mode pair $3 \leftrightarrow 6$ but the FEPE simulation showed that significant coupling does not occur. We should take a closer look at the conditions described in Section 3.1 to determine if and why they break down in this case.

The key assumtion from Section 3.1 is that the coupling coefficient $R_{nm}(r)$ can be expressed as a linear function of the internal wave displacement $\eta(r)$,

$$R_{nm}(r) = \hat{R}_{nm}\eta(r). \tag{4.1}$$

This can be true only if the integral function for $R_{mn}(r)$,

$$R_{mn} = \frac{1}{\sqrt{k_m k_n}} \int dz \frac{\omega^2}{c_o^2} \frac{\delta c(r,z)}{c_o(z)} Z_n(z) Z_m(z), \tag{4.2}$$

varies linearly with the internal wave amplitude η, which enters the equation through the sound speed perturbation term $\delta c(z,r)$. Let's examine the conditions under which this response will be linear.

Figure 4-6 shows the sound speed perturbation from an internal wave with amplitude $\eta = 5$ meters. In Section 3.1 we simply substituted the value $\delta c(z) = \delta c_{max}$ (in this case about -7 m/s) and integrated from $h_1 = 10$ meters to $h_2 = 30$ meters. This is a reasonable approximation for small internal wave displacements, but for internal waves with amplitudes larger than one or two meters the approximation can break down disasterously as shown in Figure 4-7.

The plot on the left shows the integrand from Equation 4.2 for internal wave displacements η from 0 to 10 meters in steps of 2.5 meters. The plot on the right

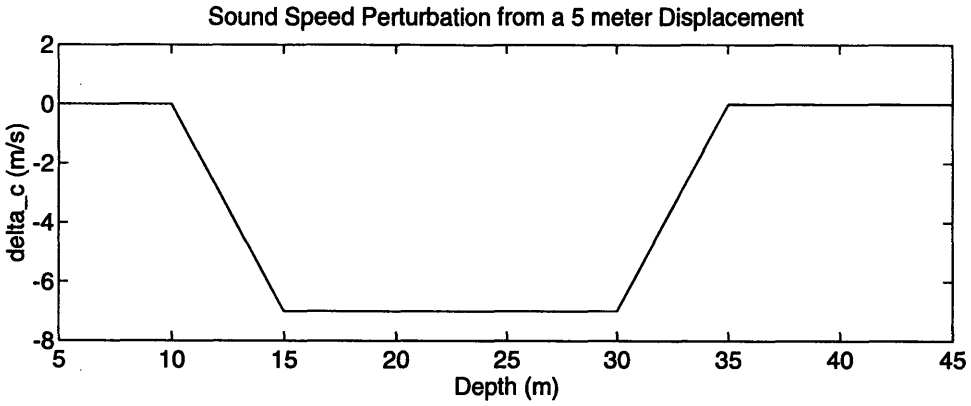

Figure 4-6: Sound Speed Perturbation by an Internal Wave

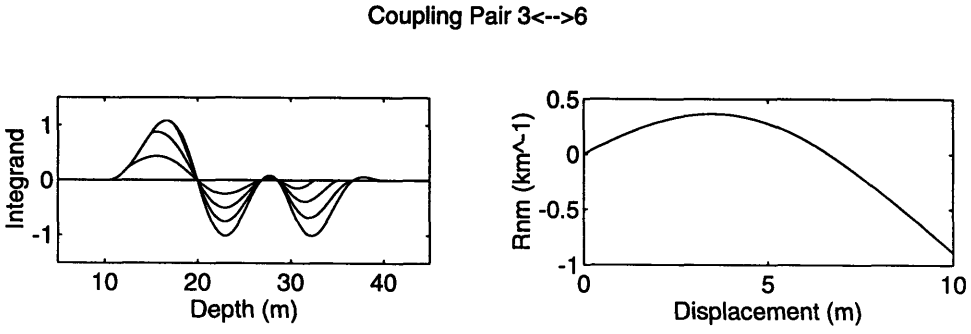

Figure 4-7: Non Linear Response of R_{nm} Integral

shows R_{nm} as a function of η. R_{nm} varies linearly with η for the first few meters but turns and curves downward before reaching $\eta = 5$ meters. This non-linear behaviour invalidates the assumption in Equation 4.1 and the Fourier Transform analysis cannot be applied in this case.

In contrast, for the first three mode pairs in Table 4.1 the Fourier Transform anaysis correctly predicted the coupling as pictured in Figures 4-2 through 4-4. For these mode pairs R_{nm} varies approximately linearly with internal wave displacement η, as Figure 4-8 shows, and we see the same wavenumber and packet length resonance characteristics that we examined in Chapter 3. The difference is that for the three

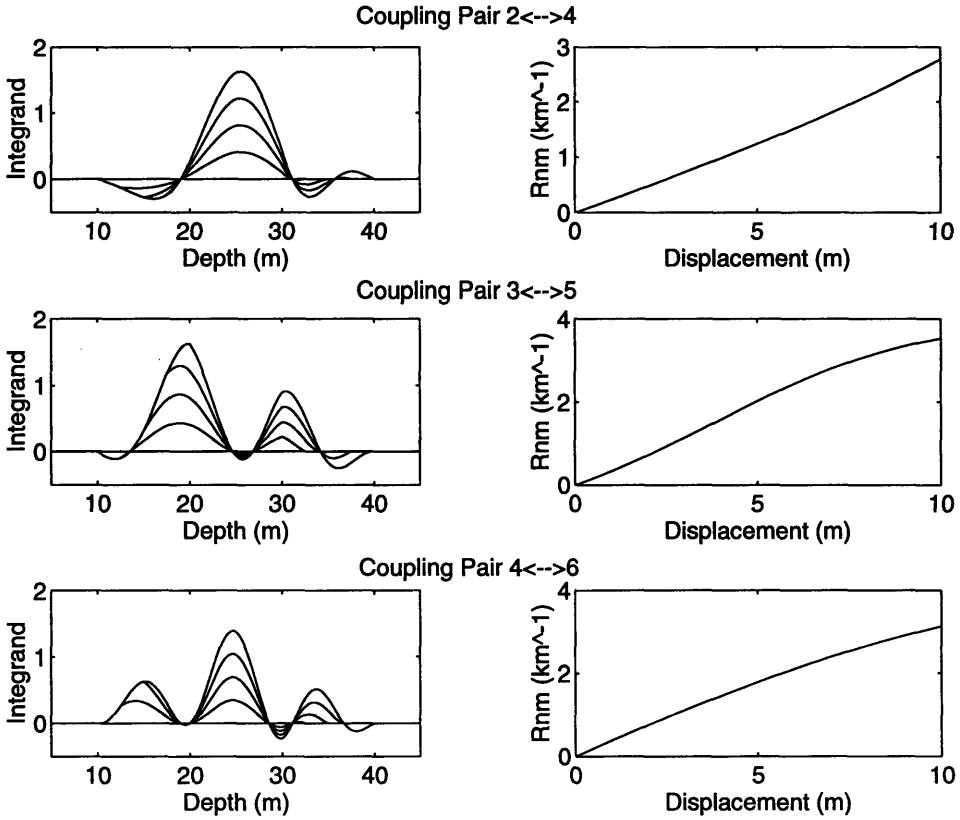

Figure 4-8: Approximately Linear Response of R_{nm} Integral

correctly predicted mode pairs the main contribution of the integrand occurs in the interior of the integration interval. For the mode pair $3 \leftrightarrow 6$, which we incorrectly predicted would generate couplng, the integrand nearly cancels over the interval $h_1 = 10$

meters to $h_2 = 30$ meters and the integral is very sensitive to the contribution beyond h_2 which grows both in amplitude and extent with the internal wave displacement η.

4.4 Effects of Internal Wave Shape

Figures 4-2 to 4-4 also showed the effect of changing the internal wave shape from a sine to the hyperbolic secant shape predicted by the hydrodynamic theory. Figure 4-1 showed these internal wave displacement functions and Figure 4-9 below shows the associated fourier transform amplitudes.

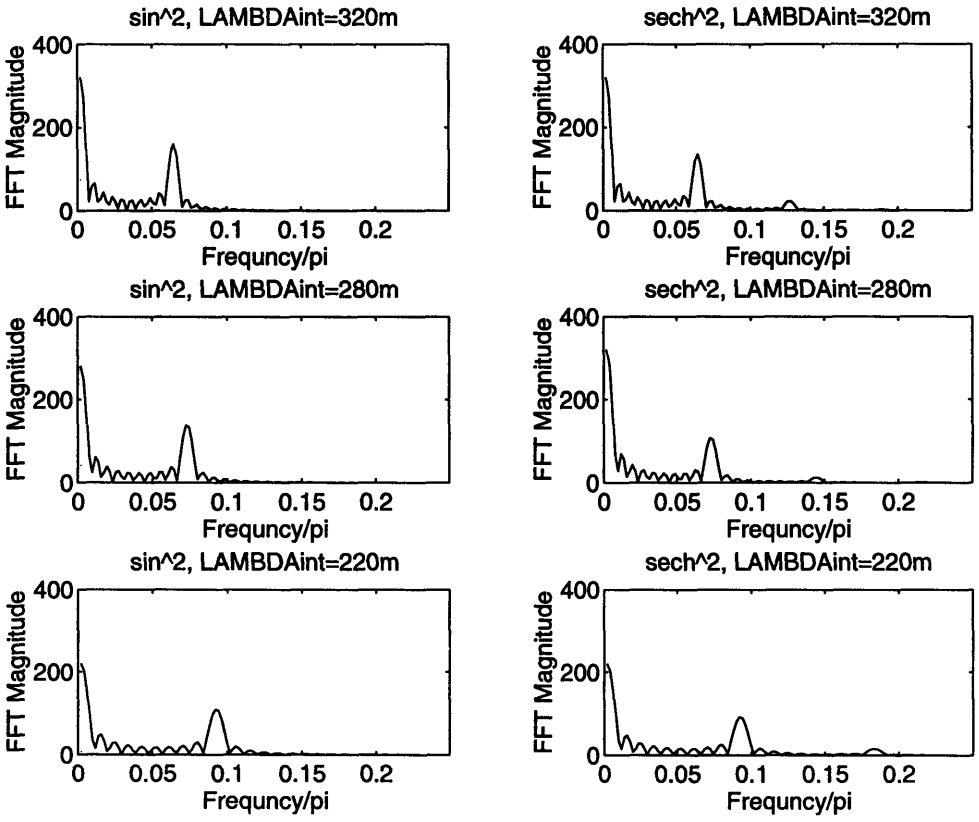

Figure 4-9: Fourier Transforms for Various Internal wave Disturbances

The transforms show that the two wave shapes have very similar frequency content, with high amplitudes at DC and the fundamental frequency for both shapes and a small contribution from the first one or two harmonics for the hyperbolic secant. Considering the wavenumber resonance analysis of Section 3.1 we would expect

strong coupling to occur for both wave shapes as long as the fundamental frequency of the wave spacing in the packet λ_{int} matches the mode difference frequency λ_{mn} for the mode pair $m \leftrightarrow n$. Figures 4-2 through 4-5 verify this.

The packet length resonance lengths λ_{PL} observed in Figures 4-2 through 4-4 do show some discrepancy in that the observed sech^2 λ_{PL}s are significantly longer than those for the $\sin^2$ waves. A closer examination of Figure 4-1 suggests a reason. Adding ten individual sech^2 waves with long tails to form the wave packet causes the displacement function to stay above zero in the troughs between wave peaks. Thus the true peak-to-trough amplitude of the wave packet is effectively reduced and a corresponding increase in packet length resonance length can be expected.

4.5 Randomized Wave Packets

We also ran simulations on randomly spaced and sized sech^2 packets. Our first example is a case where there is zero coupling response. We show this in Figure 4-10. Next we have a case where more regular coupling is going on. We show this in Figure 4-11. In both cases we see the randomization essentially distorts the fourier transform amplitudes slightly. The resulting coupling is very similar to that observed for the regularly spaced sech^2 packets.

4.6 Time Series Results

We now present a set of data which would be generated from an open water experiment similar to that shown in Figure 1-1. We consider the source (range = 0) to be the position of the feedback array and we have located the receiver array 5 km downrange. We then allow a packet of 12 7.5 meter amplitude sech^2 waves spaced at 300 meters to propagate moving at 1 m/s starting from behind the source moving downrange on a line between source and receiver and finally beyond the receiver. Figure 4-12 shows the modal energy content produced by FEPE at the receiver array for each time step. The time between steps is 54 seconds.

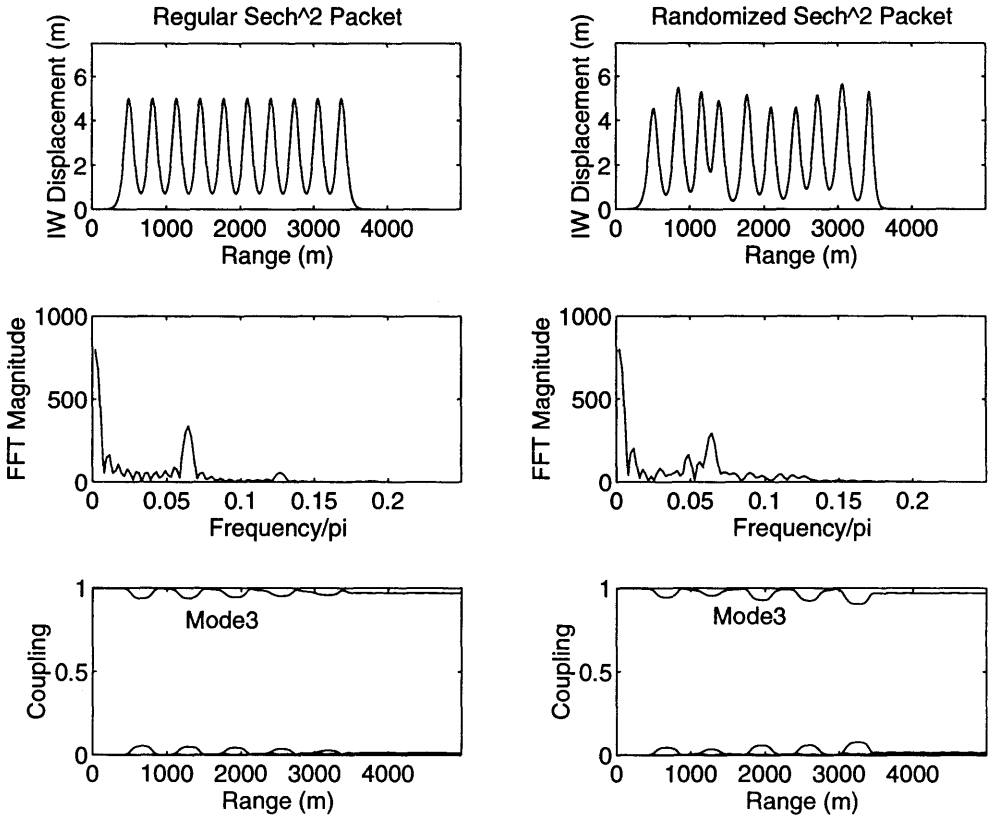

Figure 4-10: Randomized sech^2 Wave Packet — No Coupling Case

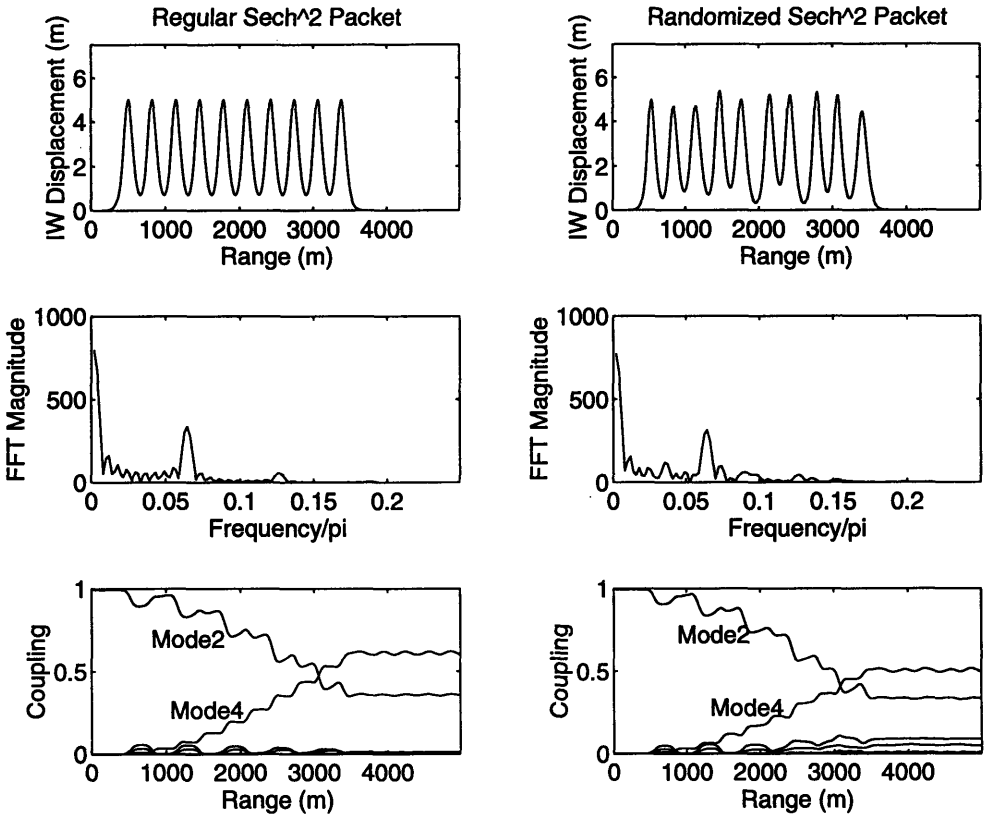

Figure 4-11: Randomized sech^2 Wave Packet — Regular Coupling

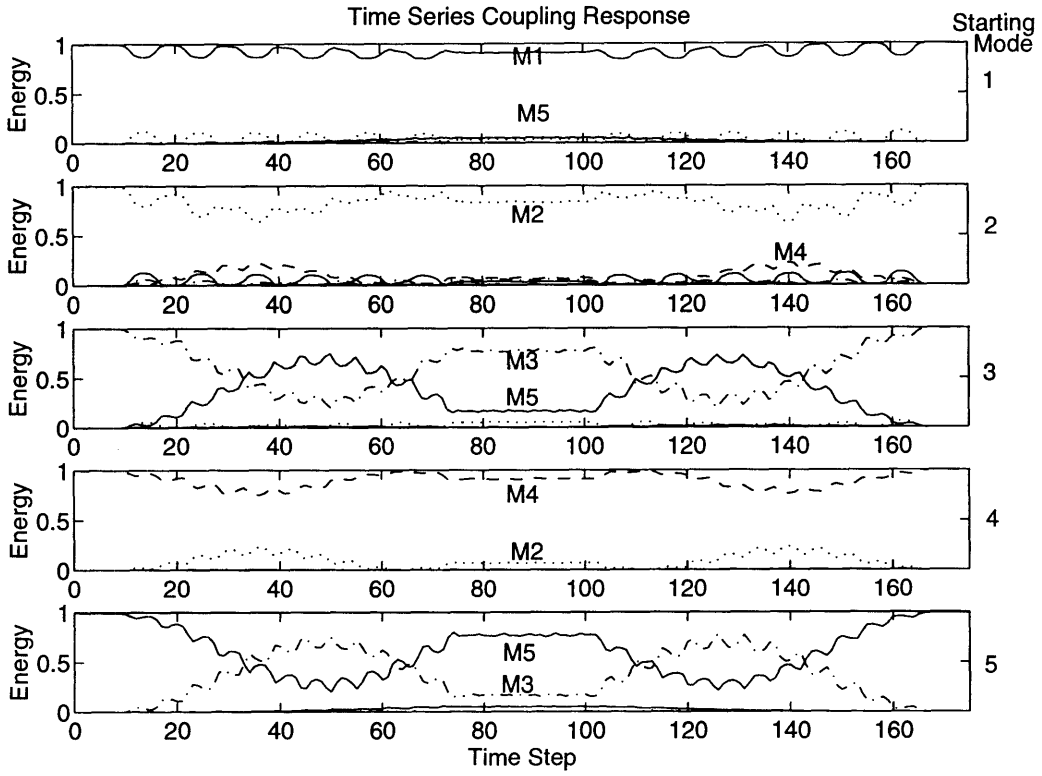

Figure 4-12: Simulated Experimental Data

In the third and fifth plots of Figure 4-12 we see the familiar exchange of energy between two modes, in this case modes 3 and 5. From Table 3.1 the modal difference wavelength is 281.6 meters, close to the internal wave spacing of 300 meters. We can also see the smaller peaks on this curve corresponding to each wave peak — we can actually count the waves as they pass the source into the space between the source and receiver. We can use this to determine the velocity of the wave fronts from the number of samples between peaks and the previously determined peak spacing. Finally we can use the observed packet length resonance length to amplitude of the wave peaks in the packet.

The second and fourth plots in Figure 4-12 also show the now familiar coupling pattern between modes 2 and 4, which have a mode difference wavelength of 311.7 meters. However, the coupling is not nearly as complete as we saw in the mode $3 \leftrightarrow 5$ case. That is, the energy transfer from the starting mode to its mode coupling pair is only about one quarter at the greatest, while in the mode $3 \leftrightarrow 5$ case almost three quarters of the energy is transferred and in the small amplitude experiments from Section 3.2 we saw virtually one hundred percent transfer of energy. Wy this happens is not clear.

The first plot from Figure 4-12 shows another unexplained mode coupling feature — a high frequency, low amplitude coupling between mode 1 and the adjacent mode number 2. The second lpot also shows this for mode 2 into modes 1 and 3.

Finally we should point out the very slow exchange of energy between modes 1 and five in the first and last plots. The mode difference wavelength is 151.2 meters, corresponding to the second harmonic of the wave spacing frequency. The presence of the second harmonic of the sech^2 function is most likely causing this very slow energy transfer.

Chapter 5

Conclusions and Future Work

We have shown that for internal wave packets of the size and type we expect to see near our experimental area that significant coupling can occur in ranges of only a few kilometers. By significant here we mean that *all* the energy from one mode can be completely transferred to another.

We also showed that the resulting coupling pairs are predictable, even for high-amplitude waves as long as we have good environmental information to determine the mode coupling coefficients R_{nm}. In addition, we showed how the interaction length of a coupled mode pair varies with wave amplitude and the particular modes involved.

Lastly we showed the kind of observed coupling which would be recorded in an experimental deployment due to the passage of an internal wave packet. We showed how this data could be used to determine the average parameters of this wave packet, including the amplitude, spacing, length, and speed of the wave packet.

In theoretical work, the completeness of the energy transfer and the high frequency, low amplitude coupling between adjacent modes still needs to be explained. Adding noise to the environment and scattering from surface waves and fine structure could also be added.

As we mentioned previously, the first open water experiment in this research program is planned for October 1994. In this experiment we will have only a source and a feedback array, with no provision for observing the coupling occuring downrange from the feedback array. We can still look for evidence of internal wave activity

through the time variation of the source weights required to maintain a single mode at the feedback array.

The next step will be to include downrange observations of the type shown in Figure 4-12. Then we can determine whether the purity of the starting mode and the level of noise and scattering in the real ocean environment will be sufficient to allow detection and parameterization of the internal wave packets travelling between the source and receiver.

Appendix A

Derivation of Coupled Mode Equations

We present a detailed derivation of the coupled mode equations with careful attention to what approximations are made and when.

We start with the Helmholtz equation, a reduced form of the wave equation which assumes a $e^{-i\omega t}$ time dependence,

$$\nabla^2 P(\mathbf{r}) + \frac{\omega^2}{c(\mathbf{r})^2} P(\mathbf{r}) = 0. \tag{A.1}$$

Here $P(\mathbf{r})$ is the acoustic pressure and $c(\mathbf{r})$ is the sound speed at the point $\mathbf{r}$. The density is assumed constant throughout the water column and the bottom with a discontinuity between the two layers. Of course this cannot be true because internal waves are caused and propagate on density gradients in the water column, but as far as the acoustics are concerned it is a good approximation.

We are considering a cylindrically symmetric problem. Expand the laplacian in terms of the cylindrical coordinates r, z, ϕ, assume ϕ independence, and substitute $p = \sqrt{r}P$ to account for cylindrical spreading,

$$\frac{\partial^2}{\partial r^2} p(r,z) + \frac{1}{4r^2} p(r,z) + \frac{\partial^2}{\partial z^2} p(r,z) + \frac{\omega^2}{c(r,z)^2} p(r,z) = 0, \tag{A.2}$$

and in the far field we can neglect the $1/r^2$ term. We treat $c(r,z)$ as the sum of a mean or base profile $c_o(z)$ and a deterministic disturbance to this profile $\delta c(r,z)$ caused by the travelling internal waves. Next we assume that $p(r,z)$ can be expressed as a sum over the discrete propagating modes of the mean profile,

$$p(r,z) = \sum_n A_n(r) Z_n(z) \tag{A.3}$$

where the $Z_n(z)$ satisfy

$$\frac{\partial^2}{\partial z^2} Z_n(z) + (\frac{\omega^2}{c_o^2(z)} - k_n^2) Z_n(z) = 0 \tag{A.4}$$

with

$$\int dz Z_n(z) Z_m(z) = \delta_{nm}$$

Here we have neglected two things. First, we have neglected the contribution due to the continuous modes of the base waveguide. Thus we no longer have a complete orthonormal set capable of representing any arbitrary pressure field. Second, we have assumed that this truncated modal sum can be used to represent the perturbed sound field caused by the internal wave perturbations.

Our next step is to substitute the mode sum A.3 into the helmholtz equation A.2. We also use the binomial expansion to approximate $(c_o + \delta c)^{-2} \approx c_o^{-2}(1 - 2\delta c/c_o)$ to get,

$$\sum_n \frac{\partial^2 A_n}{\partial r^2} Z_n + A_n \frac{\partial^2 Z_n}{\partial z^2} + \left[\frac{\omega^2}{c_o^2} \left(1 - 2\frac{\delta c}{c_o} \right) + k_n^2 - k_n^2 \right] A_n Z_n = 0.$$

We can eliminate the terms which satisfy the mode equation A.4 and apply the operator $\int dz \{\bullet\} Z_m(z)$ to obtain a differential equation for the A_n's

$$\frac{\partial^2}{\partial r^2} A_m(r) + k_m^2 A_m(r) = \sum_n \rho_{nm}(r) A_n(r) \tag{A.5}$$

with

$$\rho_{nm} = \int dz \frac{2\omega^2}{c_o^2} \frac{\delta c(r,z)}{c_o(z)} Z_n(z) Z_m(z) \tag{A.6}$$

Notice that the matrix ρ_{mn} is real (we have assumed real mode eigenfunctions Z_n)

and symmetric.

Next we specify the following form for A_m,

$$A_m(r) = \frac{1}{\sqrt{k_m}}\left[A_m^+(r)e^{ik_m r} + A_m^-(r)e^{-ik_m r}\right]. \tag{A.7}$$

A_m^+ and A_m^- represent forward and backward travelling mode shapes respectively, consistent with the assumed $e^{-i\omega t}$ time dependence. Since we have introduced a pair of complex functions we may prescribe one additional relation for the pair. We take this to be [24],

$$e^{ik_m r}\frac{dA_m^+}{dr} + e^{-ik_m r}\frac{dA_m^-}{dr} = 0 \tag{A.8}$$

Now we substitute A.7 into A.5 and use A.8 to get,

$$i\sqrt{k_m}\left[\frac{\partial A_m^+}{\partial r}e^{ik_m r} - \frac{\partial A_m^-}{\partial r}e^{-ik_m r}\right] = \sum_n \frac{1}{\sqrt{k_n}}\left[A_n^+(r)e^{ik_n r} + A_n^-(r)e^{-ik_n r}\right]\rho_{mn}$$

If we again make use of A.8 on the left hand side of this equation then we get the system,

$$\frac{\partial A_m^+}{\partial r} = -\frac{i}{2\sqrt{k_m}}\sum_n \rho_{mn}\frac{1}{\sqrt{k_n}}\left[A_n^+ e^{i(k_n-k_m)r} + A_n^- e^{-i(k_n+k_m)r}\right]$$

$$\frac{\partial A_m^-}{\partial r} = \frac{i}{2\sqrt{k_m}}\sum_n \rho_{mn}\frac{1}{\sqrt{k_n}}\left[A_n^+ e^{i(k_n+k_m)r} + A_n^- e^{-i(k_n-k_m)r}\right]$$

Now we make a forward scattering approximation. We assume that the rapidly varying terms on the right with $(k_n + k_m)$ in the complex exponential can be averaged out of these equations [25]. Then the system decouples. This is effectively the same as neglecting all the backward traveling A_n^- terms (but *not* their derivatives $\partial A_n^-/\partial r$), hence the name forward scattering approximation.

If we assume initial conditions with all the energy in the A_m^+ and none in the A_m^- then we are left with,

$$\frac{\partial A_n^+}{\partial r} = -i\sum_n \frac{1}{2\sqrt{k_m k_n}}A_n^+ e^{i(k_n-k_m)r}\rho_{mn}.$$

Letting $\psi_m = A_m^+$ yields the coupled mode equations,

$$\frac{\partial \psi_m}{\partial r}(r) = -i \sum_n \psi_n(r) R_{mn}(r) e^{ik_{mn}r}, \tag{A.9}$$

with

$$R_{mn} = \frac{\rho_{mn}}{2\sqrt{k_m k_n}} = \frac{1}{\sqrt{k_m k_n}} \int dz \frac{\omega^2}{c_o^2} \frac{\delta c(r,z)}{c_o(z)} Z_n(z) Z_m(z),$$

$$k_{mn} = k_n - k_m.$$

These equations are equivalent to those derived by Kohler and Papanicolaou [24] and Dozier and Tappert [25]. These equations emphasize perturbations to the environment and are particularly useful for studying internal wave disturbances. The local-mode based approach pioneered by Pierce [14] and Milder [15] and developed by Desaubies [21], Evans [16], and others emphasizes the adiabaticity of the environment and is better suited to applications such as slowly varying or step-wise varying bathymetry.

These are the equations on which we base most of the thesis discussion. To review the approximations made: far field approximation in Helmholtz equation, neglecting the modal continuum from the mode sum, and the forward scattering approximation.

Bibliography

[1] John Buck. PhD thesis proposal. MIT/WHOI Joint Program, 1994.

[2] Christopher Garrett and Walter Munk. Space-time scales of internal waves. *Geophysical Fluid Dynamics*, 2:225–264, 1972.

[3] Loren R. Haury, Melbourne G. Briscoe, and Marshall H. Orr. Tidally generated internal wave packets in Massachusetts Bay. *Nature*, 278:312–317, 1979.

[4] David Halpern. Observations on short-period internal waves in Massachusetts Bay. *Journal of Marine Research*, 29:116–132, 1971.

[5] Lee-Lueng Fu and Benjamin Holt. Internal waves in the Gulf of California: Observations from a spaceborne radar. *J.Geophys.Res*, 89:2053–2060, 1984.

[6] Richard P. Trask and Melbourne G. Briscoe. Detection of Massachusetts Bay internal waves by the synthetic aperature radar (SAR) on SEASAT. *Journal of Geophysical Research*, 88:1789–1799, 1983.

[7] H. Sandstrom, J. A. Elliot, and N. A. Cochrane. Observing groups of solitary internal waves and turbulence with BATFISH and echo-sounder. *Journal of Physical Oceanography*, 19:987–997, 1989.

[8] H. H. Essen, F. Schirmer, and S. Sirkes. Acoustic remote sensing of internal waves in shallow water. *Int. J. Remote Sensing*, 4:33–47, 1983.

[9] Ji xun Zhou, Xue zhen Zhang, and Peter H. Rogers. Resonant interaction of sound wave with internal solitons in the coastal zone. *JASA*, 90:2042–2054, 1991.

[10] Dietrich Marcuse. *Theory of Dielectric Optical Waveguides.* Academic Press, second edition, 1991.

[11] O. S. Lee. Effect of an internal wave on sound in the ocean. *JASA*, 33:677–681, 1961.

[12] G. B. Whitham. *Linear and Nonlinear Waves.* Wiley-Interscience, 1974.

[13] M. D. Collins. *FEPE User's Guide.* Naval Ocean Research and Development Activity, October 1988. NORDA Technical Note 365.

[14] Allan D. Pierce. Extension of the method of normal modes to sound propagation in an almost-stratified medium. *JASA*, 37:19–27, 1965.

[15] D. M. Milder. Ray and wave invariants for SOFAR channel propagation. *JASA*, 46:1259–1263, 1969.

[16] R. B. Evans. A coupled mode solution for acoustic propagation in a waveguide with stepwise depth variations of a penetrable bottom. *JASA*, 74:188–195, 1983.

[17] R. D. Graves, Anton Nagl, H. Uberall, and G. L. Zarur. Range-dependent normal modes in underwater sound propagation: Application to the wedge-shaped ocean. *JASA*, 58:1171–1177, 1975.

[18] F. B. Jensen and C. T. Tindle. Numerical modeling results for mode propagation in a wedge. *JASA*, 82:211–216, 1987.

[19] C. T. Tindle, H. Hobaek, and T. G. Muir. Normal mode filtering for downslope propagation in a shallow water wedge. *JASA*, 81:287–294, 1986.

[20] F. S. Chwieroth, A. Nagl, H. Uberall, R. D. Graves, and G. L. Zarur. Mode coupling in a sound channel with range-dependent parabolic velocity profile. *JASA*, 64:1105–1112, 1978.

[21] Yves Desaubies, Ching-Sang Chiu, and James H. Miller. Acoustic mode propagation in a range-dependent ocean. *JASA*, 80:1148–1160, 1986.

[22] Suzanne T. McDaniel. Mode coupling due to interaction with the seabed. *JASA*, 72:916–923, 1982.

[23] Suzanne T. McDaniel and Diana F. McCammon. Mode coupling and the environmental sensitivity of shallow-water propagation loss predictions. *JASA*, 82:217–223, 1987.

[24] Werner Kohler and George C. Papanicolaou. Lecture notes in physics: Wave propagation in a randomly inhomogeneous ocean. In *Wave Propagation and Underwater Acoustics*. Springer-Verlag, 1977.

[25] L. B. Dozier and F. D. Tappert. Statistics of normal mode amplitudes in a random ocean. Theory a). *JASA*, 63:353–365, 1978.